
**Showcasing research from Professor Kalyan K. Sadhu's laboratory, Department of Chemistry, Indian Institute of Technology Roorkee (IIT Roorkee), Roorkee-247667, Uttarakhand, India.**

One pot oxygen mediated syntheses of stable radicals

The stability of radicals has always been in question in the presence of $O_2$, let alone their syntheses. In this decade, $O_2$ mediated syntheses of few radical cations have been reported. In this work, syntheses of three differently substituted stable neutral radicals have been reported for the first time using $O_2$ as an electron acceptor. Cyclic radical having three C($sp^2$) atoms around the unpaired spin shows the highest thermal stability in air. Radical center substituted with two C($sp^2$) atoms and one H-atom displays distinct NMR patterns in DMSO-$d_6$ and $D_2O$.

## As featured in:


See Kalyan K. Sadhu *et al.*, *Mater. Adv.*, 2024, **5**, 1523.

ROYAL SOCIETY OF CHEMISTRY

rsc.li/materials-advances

Registered charity number: 207890

Materials Advances

ROYAL SOCIETY OF CHEMISTRY

PAPER

View Article Online
View Journal | View Issue



Cite this: *Mater. Adv.*, 2024, 5, 1523

# One pot oxygen mediated syntheses of stable radicals†

Mohit Kulshrestha,[a] C. N. Ramachandran, *[a] Rajesh G. Gonnade *[b] and Kalyan K. Sadhu *[a]

Received 17th October 2023,
Accepted 29th November 2023

DOI: 10.1039/d3ma00868a

rsc.li/materials-advances

Air- and thermally-stable emissive carbon-centered radicals (CCRs) were synthesized at room temperature in open air by varying either the base concentration or the dilution factor of the reaction mixture. The carbon radical centers in the synthesized DCP$^{\bullet}$, DCPC$^{\bullet}$ and CP$^{\bullet}$ have two adjacent C($sp^2$) in the chromenopyridine moiety and are further connected to C($sp^3$), C($sp^2$) or H atom, respectively. *In situ* generated DCPH, which contains contiguous C($sp^3$)–H bonds in chromenopyridine and dicyanomethyl moieties, is responsible for the base- and oxygen-mediated synthesis of these CCRs. Among these radicals, DCPC$^{\bullet}$ having a π-tetramer in its crystal structure shows temperature-dependent electron paramagnetic resonance (EPR) in the solid state. CP$^{\bullet}$ behaves differently in the NMR solvents DMSO-$d_6$ and $D_2O$ producing nonaromatic and aromatic species, respectively. In water, CP$^{\bullet}$ generates kinetically controlled green-red dual emissive cationic species CP(KC)$^{+}$, which showed pH-dependent reversible absorbance and fluorescence ON–OFF patterns through neutral CP–H.

## Introduction

Persistent and isolable organic CCRs, which can tolerate air and water, are always directly bound either by sp or $sp^2$ hybridized carbon atoms or by heteroatoms at adjacent sites.[1] Prominent examples of such CCRs have been observed only in the last decade.[1,2] Supramolecular host–guest interactions accommodate the air stable radical cationic dimers of tetrathiafulvalene as guests in the catenane host[2a] and radical anions as guest ligands[2b] within a metal–organic framework. Zwitterionic tetrathiafulvalene dicarboxylate radical shows metallic conduction behavior even at low temperatures.[2c] Radical stabilization in an aqueous medium has also been achieved through Zn(II)-metalloprotein containing the semiquinone radical anion.[2d] Stable organic biradicals show photothermal activity for solar-driven water evaporation.[2e] The stability of CCRs depends on the temperature and substitution around the radical center. Dicyanomethyl radicals, which are connected to two neighboring sp and one $sp^2$ hybridized carbon atoms, show temperature-dependent radical pairing either through σ or π interactions.[2f–i] CCRs, which are surrounded with neighboring $sp^3$ hybridized carbon atoms, participate as intermediates in C($sp^3$)–C($sp^3$) σ bond synthesis.[3]

In general, most of these stable radicals are not emissive owing to the presence of a single unpaired electron in SOMO. However, there are a few reports on CCRs that show emission in non-aqueous media. Substituted triphenylmethyl radicals or mono-, bis- and tris-pyridyl/phenyl-methyl radicals are emissive in either solid state or solvents with the polarity range between toluene and dichloromethane.[3] The radical anion of carbazole together with its isomer as indole-based radical cation result in charge separated phosphorescence.[4] Scanning tunneling microscopy has been utilized to measure solid state fluorescence of a single zinc-phthalocyanine radical cation adsorbed on a NaCl-covered Au(111) sample.[5] Mechanical stress induced C($sp^3$)–C($sp^3$) bond cleavage produces pink colored C($sp^2$) attached CCR with yellow emission.[6] Among heme metabolites, the tripyrridione radical shows red luminescence in THF.[7] Recently boron-stabilized CCR results in a sufficiently high quantum yield ($\phi > 0.70$) in nonpolar toluene as well as polar acetone solvents.[8] In argon-saturated cyclohexane, the azaxanthone ketyl radical having an adjacent O–H bond shows very weak fluorescence ($\phi = 0.05$) using flash photolysis.[9]

Synthetic routes for all these CCRs involve either photochemical, electrochemical or reagent-based oxidation reactions.[1–10] Despite being an oxidizing agent, oxygen generates unstable CCRs as reaction intermediates during syntheses.[10,11] Recently, Tang and coworkers synthesized oxygen-mediated radical cations from pyrrole-substituted derivatives (Scheme 1a and b).[12] However, to the best of our knowledge, there is no report of oxygen-mediated synthesis of air and thermally stable neutral organic radicals. Immediate separation of this reactive oxygen species would be one of the potential ways to overcome the limitation of air-stable CCR synthesis. We have isolated

[a] *Department of Chemistry, Indian Institute of Technology Roorkee, Roorkee–247667, Uttarakhand, India. E-mail: ramcn@cy.iitr.ac.in, sadhu@cy.iitr.ac.in*

[b] *Physical and Materials Chemistry Division, CSIR-National Chemical Laboratory, Pune–411008, Maharashtra, India. E-mail: rg.gonnade@ncl.res.in*

† Electronic supplementary information (ESI) available. CCDC 2211819. For ESI and crystallographic data in CIF or other electronic format see DOI: https://doi.org/10.1039/d3ma00868a

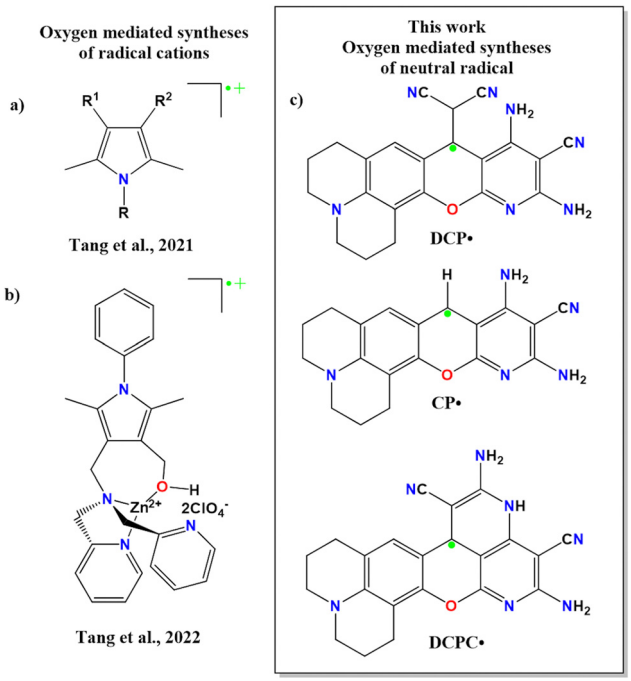


Scheme 1 Oxygen-mediated syntheses of (a), (b) pyrrole-based radical cations and (c) neutral radicals.

three neutral radicals (Scheme 1c) by tuning the base and solvent in the presence of oxygen. Till date, to the best of our knowledge, there is no report of stable organic radicals in the solid state and these molecules show diamagnetic NMR in the solution state. In this work, we are establishing such observation for the first time along with a detailed analysis of both the phases.

In this study, we have attempted to synthesize a fluorescent dye similar to our previous study (Scheme 2a)[13] by changing the active methylene-based ester to malononitrile and a differently substituted salicylaldehyde (Scheme 2b). Fortuitously, we have obtained emissive radicals as a precipitate from the room temperature one-pot reaction between 3 : 1 malononitrile and 8-hydroxyjulolidine-9-carboxaldehyde (julolidine hereafter) with piperidine as a base in ethanol. The careful analysis confirmed the oxygen-mediated synthesis of thermally and air-stable emissive DCP• (Scheme 2c) in the reaction mixture. By changing the base concentration or the solvent in other batches of the reaction mixture, emissive CP• or DCPC• were obtained (Schemes 2d and 2e). Interestingly, upon the addition of the CP• radical in water, one electron was released to generate green-red dual emissive kinetically controlled cation $CP(KC)^+$ species (Scheme 2f), which showed pH-dependent reversible absorbance and fluorescence ON–OFF patterns through neutral molecules for a few cycles.

## Results and discussion

### Radical syntheses

In this study, three equivalents of malononitrile and one equivalent of julolidine are converted into an EPR-active red-colored precipitate in the presence of a base. Piperidine as a base was added to the solutions containing malononitrile and julolidine at different strengths in ethanol (Table S1, ESI†). Stirring of 1.80 M malononitrile and 600 mM julolidine in the reaction mixture with 30 mM piperidine in 5 mL ethanol for 2 h in air produced red precipitate of DCP• (Scheme 2c). Addition of 3.0 equivalent of TEMPO, the scavenger for the superoxide dismutation reaction,[14] partially inhibits the radical synthesis

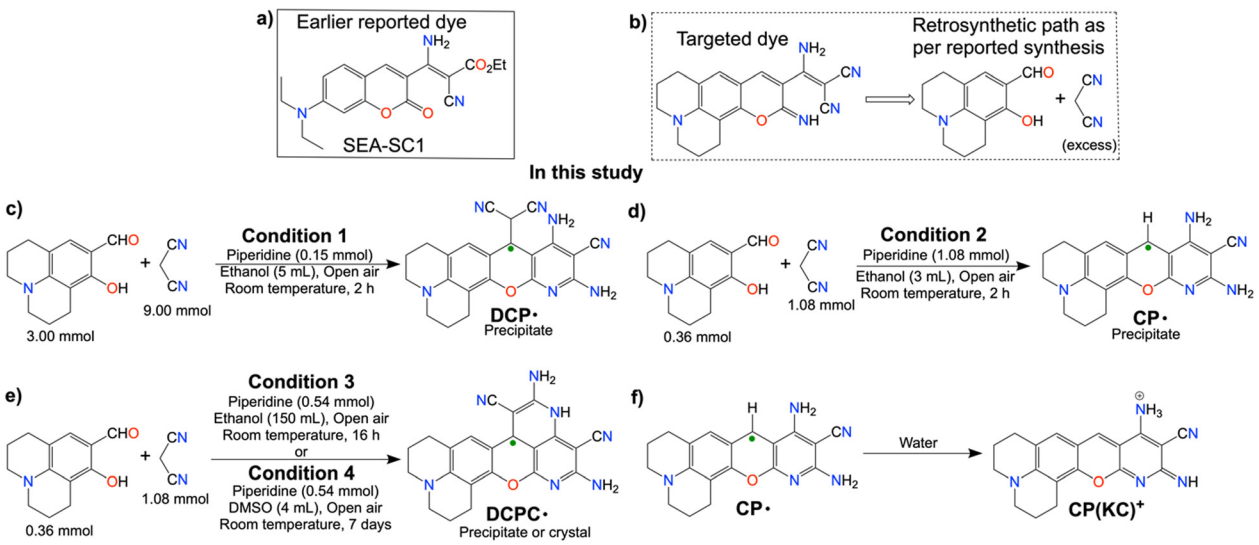


Scheme 2 (a) Previously reported fluorescent dyes from our lab; (b) targeted synthesis of fluorescent dye by replacing the active methylene compound; (c)–(e) current study for the emissive radical synthesis: one pot room temperature synthesis of (c) DCP•, (d) CP• and (e) DCPC• by varying piperidine equivalent to two different concentrated solutions containing malononitrile and 8-hydroxy julolidine-9-carboxaldehyde either in concentrated ethanolic solution, diluted ethanolic solution or DMSO solution, and (f) conversion of CP• to the $CP(KC)^+$ cation by the addition of the radical in water.

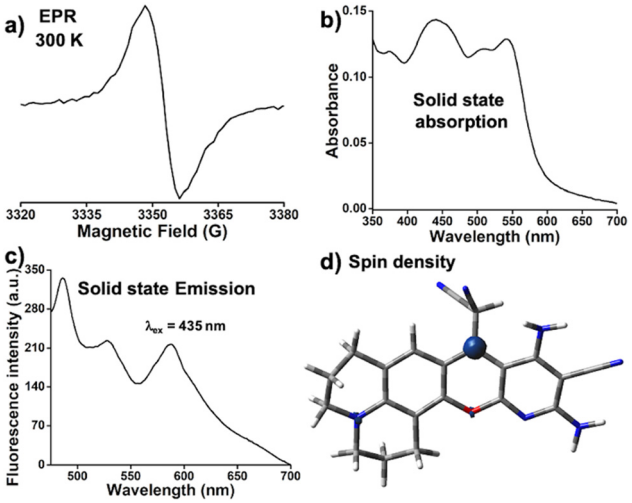


Fig. 1 DCP• radical: (a) EPR signal ($g$ = 2.00) at 300 K, solid-state (b) absorption and (c) emission ($\lambda_{ex}$ = 435 nm) of DCP• and the (d) calculated spin density of DCP•.

as it interacts mostly with the superoxide after the rapid precipitation of CCR. The role of $O_2$ in the DCP• synthesis was verified by performing the reaction in dry ethanol under continuous flow of nitrogen. Although the solution turns red due to the Knoevenagel condensation reaction, no precipitation was observed even after 4 h of the reaction. However, the same reaction precipitates DCP• within the next 15 min in the presence of air. The reaction in dry $CD_3OD$ in the absence of $O_2$ was performed to find out the condensation product, which was producing the red solution (Fig. S1, ESI†).

The reaction mixture of 360 mM malononitrile and 120 mM julolidine with 360 mM piperidine in 3 mL ethanol produces CP• as a red precipitate (Scheme 2d and Table S1, ESI†) by breaking the C($sp^3$)–C($sp^3$) bond. CP•, which is sufficiently water soluble, forms CP(KC)$^+$ cationic species (Scheme 2f) by losing one electron in water.[15] Multiple fast reactions from the hydrated electron result in hydroxide ions in the solution as the counter anion.[15]

The synthetic attempt of CP• in DMSO by lowering the base concentration results in a single crystal of yellow cyclized DCPC• (Scheme 2e) after 6 days. The same quantity of the reactants in 150 mL ethanol also produces DCPC• as the precipitate after 16 h. HRMS studies of all these three radicals show the characteristic molecular weight of the radicals (Fig. S2–S4, ESI†). 4-aminopiperidine behaves similarly to piperidine and does not affect the yields much. Radical yields were significantly lowered in the presence of 1.5 or 3.0 eq. of trimethylamine, and trimethylamine, for the reactions between 360 mM malononitrile and 120 mM julolidine in 3 mL EtOH. Aniline does not give a precipitate under both DCP• and CP• synthetic conditions. Strong bases such as DBU and tetramethyl guanidine also give comparable yields of piperidine (Table S1, ESI†).

### DCP• radical: adjacent C($sp^3$) substituted CCR

Formation of DCP• in the solid state was confirmed from the EPR signal ($g$ = 2.00), which remained unaltered within 300 K to

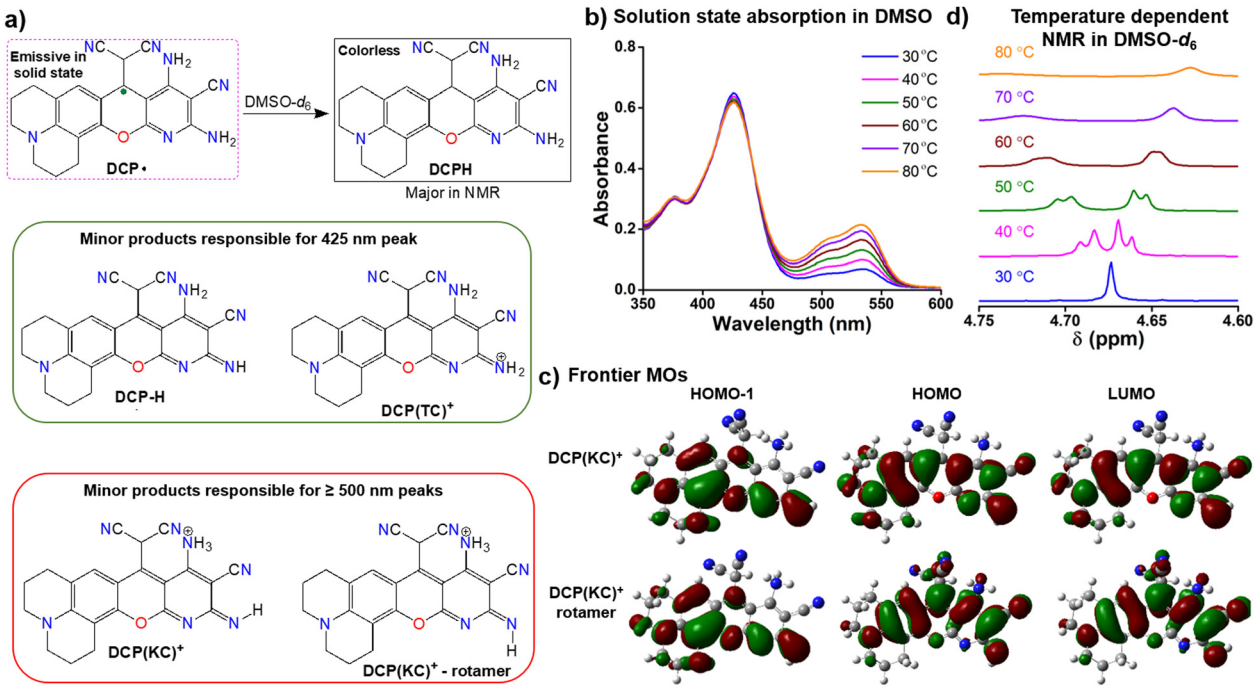


Fig. 2 DCP• radical: solution state studies and theoretical correlation. (a) A schematic representation of the speciation from DCP• in DMSO solution; (b) absorption studies of DCP• as DCP(KC)$^+$ in DMSO till 80 °C; (c) frontier molecular orbitals involved in the electronic transition for DCP(KC)$^+$ and its imine (=N–H) rotamer; (d) temperature-dependent $^1$H-NMR studies for the conversion of DCPH to DCP(KC)$^+$ till 80 °C in DMSO solution.

100 K (Fig. 1a and Fig. S5, ESI†). The solid state $^{1}$H and $^{13}$C NMR (Fig. S6, ESI†) of DCP$^{\bullet}$ show broad peaks. The thermal stability study of DCP$^{\bullet}$ in air showed no decomposition up to 140 °C (Fig. S7, ESI†). The visible region absorption of DCP$^{\bullet}$ in the solid state showed peaks at 435 nm, 510 nm, and 545 nm (Fig. 1b). The radical shows three emission peaks at 495 nm, 520 nm, and 595 nm (Fig. 1c, $\phi_{abs}$ = 0.71) in the solid state by exciting the sample at 435 nm. Theoretical studies were carried out on both DCP$^{\bullet}$ and CPD$^{\bullet}$ (Fig. S8, ESI†) with radical centers on couminopyridine (CP) and dicyanomethyl (D) moieties, respectively, to identify the radical center. Comparison of TDDFT (Fig. S9, ESI†) results with the experimental absorption study confirmed the formation of DCP$^{\bullet}$, where calculated spin density is mostly localized on the carbon center (Fig. 1d).

Among the common organic solvents, DCP$^{\bullet}$ is only soluble in DMSO and DMF, but both solutions showed no EPR signal (Fig. S10, ESI†). The NMR study of DCP$^{\bullet}$ in DMSO-$d_6$ showed diamagnetic NMR (Fig. S11, ESI†) due to the formation of DCPH (Fig. 2a) by the overall abstraction of the hydrogen atom from the solvent. Poor EPR signal (Fig. S12, ESI†) was observed immediately after the addition of DCP$^{\bullet}$ in DMSO due to the formation of DMSO radicals, which disappeared with time (Fig. S10, ESI†). A few minor peaks in NMR were present due to the degradation of the DMSO-$d_6$ radical (Fig. S13, ESI†). Other substituted DCPH syntheses were reported without any radical formation.[16] The DCP$^{\bullet}$ radical in DMSO was confirmed by observing EPR in the presence of the spin-trapping agent DMPO at 100 K. (Fig. S14a, ESI†). Furthermore, the NMR of DCP$^{\bullet}$ was taken in the presence of DMPO in DMSO-$d_6$ at room temperature, it was observed broad, and one of the characteristic peaks was diminished due to the adduct formation of DMPO with DCP$^{\bullet}$. (Fig. S15, ESI†)

The reaction was carried out at the NMR scale in DMSO-$d_6$ to understand the reaction pathway. During the reaction, two characteristic peaks corresponding to C($sp^3$)–H for the *in situ* generated DCPH (Fig. S16, ESI†) were observed. The presence of organic base and oxygen is responsible for the conversion of DCPH to DCP$^{\bullet}$ as per the reported method.[17] Theoretical studies predict the synthetic route of DCP$^{\bullet}$ from the *in situ* generated DCPH through the base-mediated synthesis of CPD$^{-}$, followed by a single electron transfer to oxygen and radical center conversion to energetically favorable DCP$^{\bullet}$ (Fig. S17 and S18, ESI†). The high energy barrier for the conversion of CPD$^{-}$ to DCP$^{-}$ by proton transfer (Fig. S19, ESI†) restricts the conversion *via* an alternate route. However, the energetically unfavorable ($\Delta G$ = +69.32 kcal mol$^{-1}$) process for the radical formation from DCPH is only possible due to the phase separation of DCP$^{\bullet}$ in the reaction condition.

At room temperature, the red NMR solution of DCP$^{\bullet}$ exists as DCPH form in DMSO-$d_6$. However, the TDDFT study on DCPH suggests no significant absorption in the visible region (Fig. S20, ESI†) due to a lack of π-conjugation. Absorption of the DMSO solution at 30 °C shows one major peak at 425 nm and two minor peaks at 500 and 535 nm (Fig. 2b). TDDFT studies indicate thermodynamically-controlled cation DCP(TC)$^{+}$ or neutral DCP–H (Fig. 2a) for the 425 nm absorption and kinetically controlled cation DCP(KC)$^{+}$ and its imine N–H rotamer (Fig. 2a and Fig. S21, ESI†) for the dual absorption peaks ≥500 nm.

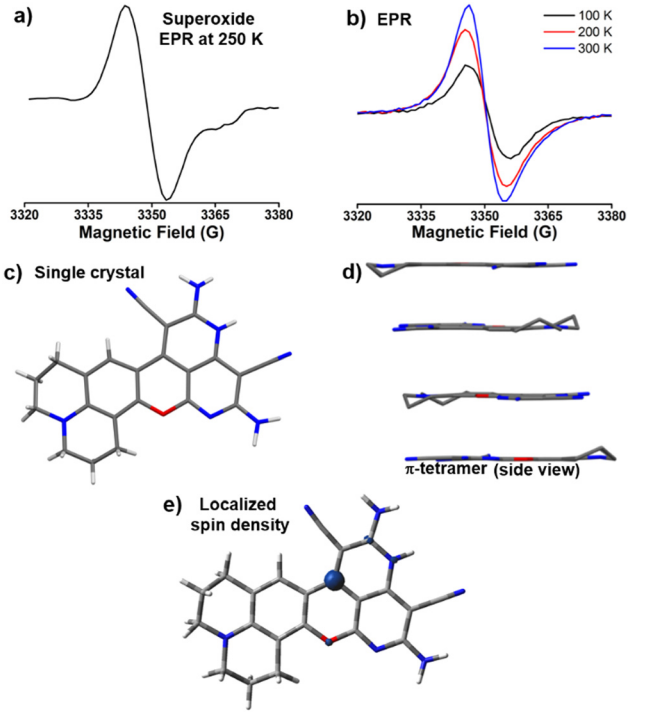


Fig. 3 DCPC$^{\bullet}$ radical: spectroscopy, crystal structure and spin density. (a) The EPR signal at 250 K for the superoxide ($g$ = 2.00) generated in DMSO solution after 6 days of the reaction with 3 : 1 malononitrile and 8-hydroxy julolidine-9-carboxaldehyde in the presence of 1.5 equivalent piperidine, (b) temperature dependent EPR signals ($g$ = 2.00) for DCPC$^{\bullet}$, (c) the DCPC$^{\bullet}$ single crystal asymmetric unit (solvent DMSO molecules are omitted for clarity), (d) side view of the π-tetramer in DCPC$^{\bullet}$ and (e) the localized spin density of DCPC$^{\bullet}$.

These cationic species originate from the radical disproportionation reaction[18] (Fig. S22, ESI†). The corresponding anion receives a proton from DMSO to form DCPH and the dimsyl anion.[19] The cationic species accepts an electron from the dimsyl anion to generate DCP$^{\bullet}$ and DMSO radicals (Fig. S22, ESI†).[20] This overall conversion produces major DCPH as confirmed in NMR (Fig. S11, ESI†). Minor cationic DCP(KC)$^{+}$ and DCP(TC)$^{+}$ or neutral DCP–H (Fig. 2a) products are responsible for coloration. The $n \rightarrow \pi^*$ and $\pi \rightarrow \pi^*$ electronic transitions within these cationic and neutral species involve HOMO−1 to LUMO orbitals (Fig. 2c and Fig. S23, ESI†).

Upon heating the DMSO solution to 80 °C, a significant increase in the absorption intensities of the two peaks ≥ 500 nm was observed (Fig. 2b). This change in the absorbance can be correlated with temperature-dependent $^{1}$H-NMR studies, where a 20% decrease in the CP-based C($sp^3$)–H peak (Fig. 2d) was observed at 80 °C due to the formation of DCP(KC)$^{+}$ species. By exciting the DMSO solution at 535 nm for DCP(KC)$^{+}$ species, dual emissions were observed at 560 nm and 600 nm ($\phi_{rel}$ = 0.56, Fig. S24, ESI†). An enhancement of the emission intensities was observed upon heating the solution (Fig. S25, ESI†).

### DCPC$^{\bullet}$ radical: three C($sp^2$) substituted CCR

A single electron transfer reaction from CPD$^{-}$ to oxygen produces the CPD$^{\bullet}$ and superoxide, which is unstable to show the

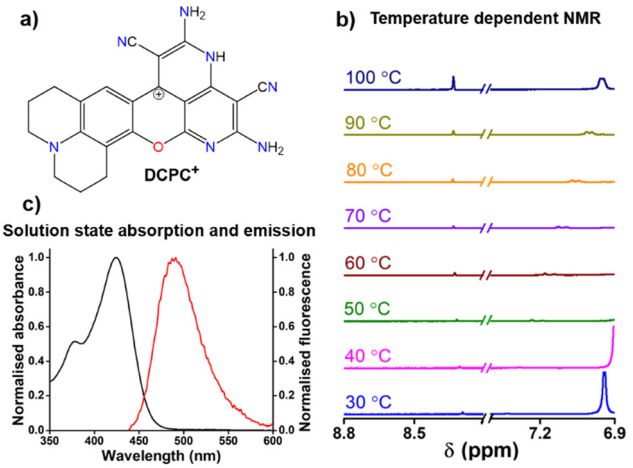


Fig. 4 (a) Chemical structure of $DCPC^+$; (b) temperature-dependent NMR data of $DCP^\bullet$ radical as DCPH in DMSO-d showing generation of new peaks due to conversion to $DCPC^+$ at high temperature; (c) normalized absorbance and emission properties of $DCPC^\bullet$ as $DCPC^+$ in DMSO.

EPR signal in ethanol. In the case of the reaction in DMSO for $DCPC^\bullet$, the filtrate shows an EPR signal (Fig. 3a) due to the high stability of superoxide in DMSO.[21] Thermal stability of $DCPC^\bullet$ in the presence of air is significantly enhanced in comparison to the recently reported highest thermally stable organic radicals[22] and $DCP^\bullet$ (Fig. S26, ESI†). Solid state NMR shows broad peaks (Fig. S27, ESI†) and a redical nature was observed in EPR (Fig. 3b).

$DCPC^\bullet$ from the DMSO reaction mixture crystallizes in orthorhombic centrosymmetric *P*bcn space group containing one molecule of $DCPC^\bullet$ (Fig. 3c) and two DMSO solvent molecules in the asymmetric unit. In the unit cell, a total of eight $DCPC^\bullet$ molecules are present. Crystal packing reveals the presence of the radical π-tetramer, which are related by screw axes and center of symmetry (Fig. 3d). The presence of screw axes between the π-tetramer generates residual non-zero electron spin, which is responsible for the EPR signal of $DCPC^\bullet$ even at 100 K (Fig. 3b). The repulsion between the unpaired electrons within π-tetramer of $DCPC^\bullet$ results in slightly higher π–π distances (~3.55 to 3.77 Å) than the reported π-tetramer[23] (3.34 Å) in *N*-butoxyphenyl(naphthalene)diimide. The temperature-dependent boost in the EPR intensities of $DCPC^\bullet$ takes place due to the enhancement of π–π distances at 300 K as observed in the reported π-tetramer.[23]

The absorbance spectrum of $DCPC^\bullet$ showed a major peak at 425 nm (Fig. S28, ESI†) with a broad emission (Fig. S29, $\phi_{abs}$ = 0.95, ESI†) in the solid state. TDDFT studies confirmed the absorbance of the radical species (Fig. S30, ESI†). Similar to the localized spin density for $DCP^\bullet$, $DCPC^\bullet$ has also localized spin density on the same carbon center (Fig. 3e). In the NMR study, unlike hydrogen abstraction for $DCP^\bullet$ at room temperature, the $DCPC^\bullet$ is soluble in DMSO-$d_6$ in hot conditions and exists as $DCPC^+$ (Fig. 4a) in diamagnetic NMR at 130 °C (Fig. S31, ESI†) and has no EPR signal (Fig. S32, ESI†). The difference in the solubility between $DCP^\bullet$ and $DCPC^\bullet$ might be due to the absence of any hydrogen adjacent to the radical position in $DCPC^\bullet$. No change in the characteristic NMR peaks in the presence of TEMPO (Fig. S33, ESI†) confirmed the cationic form in the solution instead of the radical form. EPR of $DCPC^\bullet$ in DMSO was observed in the presence of DMPO (Fig. S14b, ESI†). The temperature-dependent NMR of $DCP^\bullet$ in DMSO-$d_6$ shows the disappearance of both characteristic $C(sp^3)$–H peaks for DCPH (Fig. S34, ESI†) and the appearance of new peaks at higher temperatures due to cyclization towards $DCPC^+$ (Fig. 4b). Similar studies have been observed for the temperature-dependent absorption of $DCP^\bullet$ in DMSO at >80 °C (Fig. S35, ESI†). The solution state absorption and emission due to $DCPC^\bullet$ are obtained at 425 and 485 nm, respectively ($\phi_{rel}$ = 0.39, Fig. 4c) in DMSO. TDDFT studies (Fig. S36, ESI†) confirmed the origin of the absorption peak

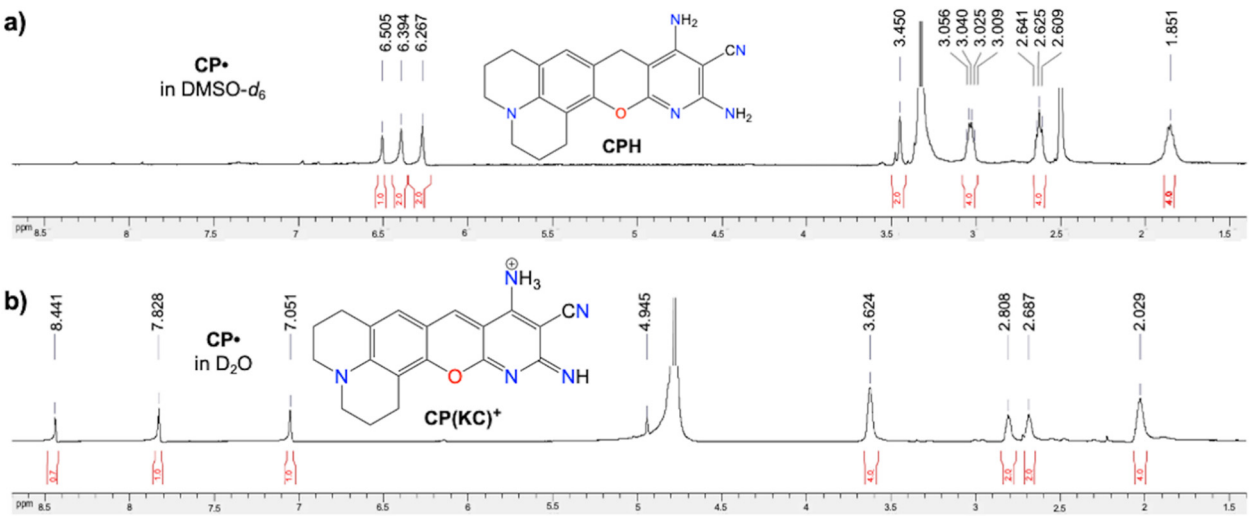


Fig. 5 $CP^\bullet$ radical: $^1H$ NMR spectra of (a) nonaromatic CPH in DMSO-$d_6$ and (b) aromatic $CP(KC)^+$ in $D_2O$.

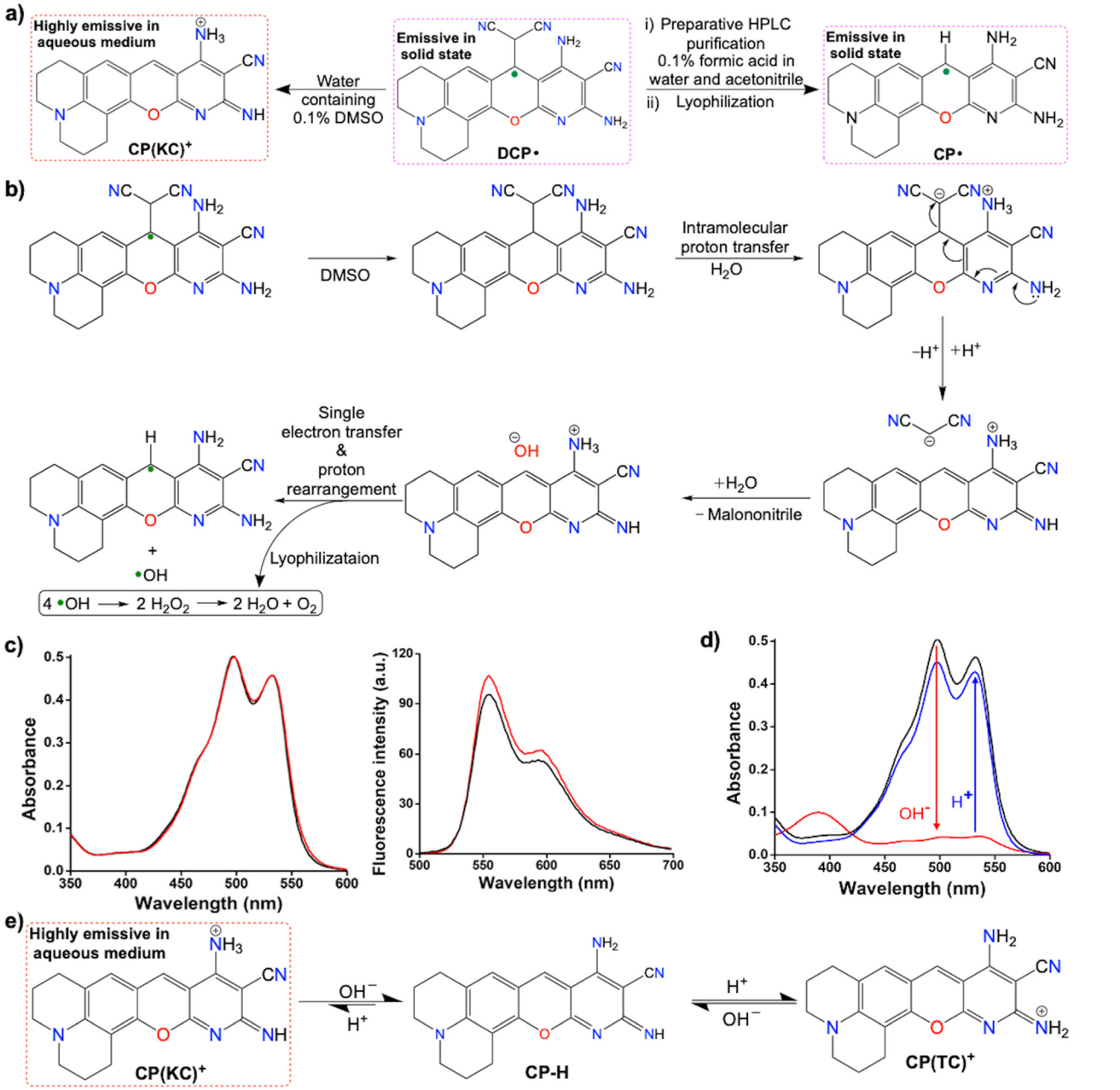


Fig. 6 CP• radical: solution state spectroscopy. (a) A schematic representation of the conversion of DCP• to CP• and CP(KC)$^+$; (b) the proposed mechanism for the water-mediated conversion of DCP• to the CP• radical *via* CP(KC)$^+$; (c) absorbance and emission of CP(KC)$^+$ obtained from 20 μM CP• in water (red) and DCP• in water containing 0.1% DMSO (black); (d) reversible acid–base cycle for the conversion of CP(KC)$^+$ and CP–H and (e) a schematic representation of equilibrium shifting between CP(KC)$^+$ *vs.* CP(TC)$^+$ and CP–H after a few rounds of deprotonation and protonation studies from CP(KC)$^+$.

for DCPC$^+$ species. However, in the aqueous medium, very weak absorption was obtained without any significant emission (Fig. S37, ESI†).

### CP• radical: H atom substituted CCR and kinetically-controlled CP(KC)$^+$ cation in water

Similar to DCP•, CP• also provides temperature independent EPR signals (Fig. S38, ESI†), typical solid-state broad peaks NMR (Fig. S39, ESI†), and solid state absorbance and emission ($\phi_{abs}$ = 0.62, Fig. S40, ESI†). However, the thermal stability of CP• in the presence of air is greater than DCP• and comparable to DCPC• (Fig. S41, ESI†) due to the absence of any C($sp^3$) atom in CP• and DCPC•. CP• also has localized spin density at the carbon centre (Fig. S42, ESI†). The solution state NMR of CP• also shows nonaromatic CPH by abstracting hydrogen from DMSO-$d_6$ (Fig. 5a and Fig. S43, ESI†). Interestingly in $D_2O$, CP• shows distinctly different diamagnetic NMR peaks (Fig. 5b and Fig. S44, ESI†) due to the formation of the CP(KC)$^+$ cationic

species. Also, EPR has been observed in DMSO in the presence of DMPO (Fig. S14c, ESI†). Nucleus-independent chemical shift calculations for all the rings containing these three new CCRs have been found to be anti-aromatic (Fig. S45, ESI†).

Color-based purification of DCP$^{\bullet}$ was performed to obtain the emissive species selectively from its DMSO solution *via* the gradient mode using the preparative HPLC with acidic water and acetonitrile combination. Surprisingly, the characterization of the lyophilized solid after purification confirmed the conversion of DCP$^{\bullet}$ to CP$^{\bullet}$ (Fig. 6a). This is due to the C–C bond cleavage in water-mediated (Fig. 6b) or base-guided heterolytic cleavage[24] (Fig. S46, ESI†) in the presence of radicals. The proposed formation of the CP(KC)$^{+}$ cationic species in the water-mediated reaction was confirmed by the change of absorption with increasing amounts of water (Fig. S47, ESI†). The presence of a clear absorbance peak at 446 nm (Fig. S48 and S49, ESI†) before the generation of the dual peak during the synthesis of CP$^{\bullet}$ indicates the formation of a CP–H intermediate due to the base-mediated breaking of the C–C bond. The emission generated from DCP$^{\bullet}$ in water containing 0.1% DMSO ($\phi_{rel}$ = 0.77, Fig. 6c) was enhanced by DCP(KC)$^{+}$ in DMSO ($\phi_{rel}$ = 0.56, Fig. S24, ESI†). The absorption ($\lambda_{abs}$ = 500 nm and 535 nm) and emission ($\lambda_{em}$ = 555 and 595 nm; $\lambda_{ex}$ = 535 nm) patterns from DCP$^{\bullet}$ in water containing 0.1% DMSO are identical to the patterns of CP$^{\bullet}$ in pure water due to the formation of CP(KC)$^{+}$ in both the cases (Fig. 6d). The TDDFT studies of the optimized CP(KC)$^{+}$ and its rotamer confirms the transition from HOMO to LUMO (Fig. S50, ESI†). The slight deviations in emission originating from DCP$^{\bullet}$ are due to the presence of 0.1% DMSO, which significantly changes the absorption (Fig. S47, ESI†). Remarkably, the absorption and emission intensities of the CP$^{\bullet}$ in the water solution containing 0.1% DMSO drastically decreased (Fig. S51, ESI†) due to the formation of non-emissive colorless CPH in DMSO (Fig. S52, ESI†).

The absorbance and emission properties of CP(KC)$^{+}$ in the aqueous medium decreased (Fig. 6d) upon the addition of the base due to the formation of neutral CP–H (Fig. 6e). The shift in the absorbance of CP–H is due to the use of a strong base. The process is reversible with ~10% loss of intensities in the presence of HCl (Fig. 6e). Fluorescence lifetime data confirm the enhancement of non-radiative decay rate constant upon the base treatment (Fig. S53 and Table S2, ESI†). Performing these acid–base reversible cycles 6 or more times, there is negligible change in the absorbance at 500 nm (Fig. S54, ESI†) and emission at 555 nm (Fig. S55, ESI†). This behavior is due to the equilibrium with the other thermodynamically-controlled CP(TC)$^{+}$ cation (Fig. 6f and Fig. S56, ESI†), which has a similar absorption pattern to neutral CP–H. The pH-dependent absorption and emission studies further show that the change of the emission profile depending upon the excitation wavelengths at highly basic pH due to the complete conversion to neutral CP–H (Fig. S57 and S58, ESI†).

## Conclusion

We exploited aerial $O_2$ unknowingly as an electron acceptor for synthesizing three distinct air-stable fluorescent CCRs. We show that neighboring C($sp^3$)–H bonds are not only involved in the radical synthesis on the chromenopyridine unit but also play a key role in the emissive property. The solvent or concentration-dependent cyclization process shows the formation of C($sp^2$) atoms stabilized second radical, which is also emissive and stabilized by the tetrameric π–π interaction in the crystal structure. The excess amount of base or water content in the reaction mixture is accountable for the production of unique one adjacent H atom stabilized third radical, which in the presence of water produces kinetically controlled green-red dual emissive cationic species. We believe that these oxygen and water-mediated air-stable fluorescent organic radical synthetic routes will open new avenues in the synthesis of fluorescent dyes. We are currently focusing on the bioimaging applications of the green-red dual-emissive cationic and radical species.

## Author contributions

K.K.S. conceived the idea and wrote the manuscript. M.K. performed the synthesis, characterization, photophysical studies, and EPR experiments. C.N.R. performed the computational studies. R.G.G. solved the crystal structure. All authors discussed the results and commented on the manuscript.

## Conflicts of interest

There are no conflicts to declare.

## Acknowledgements

K. K. S. acknowledges the DST Nanomission (DST/NM/NB/2018/237) and SERB-DST Grant (CRG/2023/001415) for research funding. M. K. acknowledges the same two funds for his fellowship. The authors thank DST-FIST (SR/FST/CS-II/2018/72(C)) India for 500 MHz NMR support. The authors also thank Prof. Nicolas Winssinger from the University of Geneva, Switzerland for the helpful discussion.

## Notes and references

1 (*a*) K. Cai, L. Zhang, R. D. Astumian and J. F. Stoddart, *Nat. Rev. Chem.*, 2021, **5**, 447; (*b*) O. Haze, B. Corzilius, A. A. Smith, R. G. Griffin and T. M. Swager, *J. Am. Chem. Soc.*, 2012, **134**, 14287.

2 (*a*) J. M. Spruell, A. Coskun, D. C. Friedman, R. S. Forgan, A. A. Sarjeant, A. Trabolsi, A. C. Fahrenbach, G. Barin, W. F. Paxton, S. K. Dey, M. A. Olson, D. Benítez, E. Tkatchouk, M. T. Colvin, R. Carmielli, S. T. Caldwell, G. M. Rosair, S. G. Hewage, F. Duclairoir, J. L. Seymour, A. M. Z. Slawin, W. A. Goddard III, M. R. Wasielewski, G. Cooke and J. F. Stoddart, *Nat. Chem.*, 2010, **2**, 870; (*b*) B. Lü, Y. Chen, P. Li, B. Wang, K. Müllen and M. Y. Lü, *Nat. Commun.*, 2019, **10**, 767; (*c*) Y. Kobayashi, T. Terauchi, S. Sumi and Y. Matsuhita, *Nat. Mater.*, 2017, **16**, 109;

(*d*) G. Ulas, T. Lemmin, Y. Wu, G. T. Gassner and W. F. DeGrado, *Nat. Chem.*, 2016, **8**, 354–359; (*e*) G. Chen, J. Sun, Q. Peng, Q. Sun, G. Wang, Y. Cai, X. Gu, Z. Shuai and B. Z. Tang, *Adv. Mater.*, 2020, **32**, 1908537; (*f*) R. Zhang, A. Ellern and A. H. Winter, *Angew. Chem., Int. Ed.*, 2021, **60**, 25082; (*g*) B. Adinarayana, K. Kato, D. Shimizu, T. Tanaka, K. Furukawa and A. Osuka, *Angew. Chem., Int. Ed.*, 2020, **59**, 4320; (*h*) K. Yang, X. Zhang, A. Harbuzaru, L. Wang, Y. Wang, C. Koh, H. Guo, Y. Shi, J. Chen, H. Sun, K. Feng, M. C. R. Delgado, H. Y. Woo, R. P. Ortiz and X. Guo, *J. Am. Chem. Soc.*, 2020, **142**, 4329–4340; (*i*) K. Okino, S. Hira, Y. Inoue, D. Sakamaki and S. Seki, *Angew. Chem., Int. Ed.*, 2017, **56**, 16597.

3 (*a*) Q. Peng, A. Obolda, M. Zhang and F. Li, *Angew. Chem., Int. Ed.*, 2015, **54**, 7091; (*b*) X. Ai, E. W. Evans, S. Dong, A. J. Gillett, H. Guo, Y. Chen, T. J. H. Hele, R. H. Friend and F. Li, *Nature*, 2018, **563**, 536; (*c*) H. Guo, Q. Peng, X. K. Chen, Q. Gu, S. Dong, E. W. Evans, A. J. Gillett, X. Ai, M. Zhang, D. Credgington, V. Coropceanu, R. H. Friend, J. L. Brédas and F. Li, *Nat. Mater.*, 2019, **18**, 977; (*d*) A. Abdurahman, T. J. H. Hele, Q. Gu, J. Zhang, Q. Peng, M. Zhang, R. H. Friend, F. Li and E. W. Evans, *Nat. Mater.*, 2020, **19**, 1224; (*e*) S. Kimura, R. Matsuoka, S. Kimura, H. Nishihara and T. Kusamoto, *J. Am. Chem. Soc.*, 2021, **143**, 5610; (*f*) K. Kato, S. Kimura, T. Kusamoto, H. Nishihara and Y. Teki, *Angew. Chem., Int. Ed.*, 2019, **58**, 2606.

4 C. Chen, Z. Chi, K. C. Chong, A. S. Batsanov, Z. Yang, Z. Mao, Z. Yang and B. Liu, *Nat. Mater.*, 2021, **20**, 175.

5 B. Doppagne, M. C. Chong, H. Bulou, A. Boeglin, F. Scheurer and G. Schull, *Science*, 2018, **361**, 251.

6 S. Kato, S. Furukawa, D. Aoki, R. Goseki, K. Oikawa, K. Tsuchiya, N. Shimada, A. Maruyama, K. Numata and H. Otsuka, *Nat. Commun.*, 2021, **12**, 126.

7 E. Tomat and C. J. Curtis, *Acc. Chem. Res.*, 2021, **54**, 4584.

8 M. Ito, S. Shirai, Y. Xie, T. Kushida, N. Ando, H. Soutome, K. J. Fujimoto, T. Yanai, K. Tabata, Y. Miyata, H. Kita and S. Yamaguchi, *Angew. Chem., Int. Ed.*, 2022, **61**, e202201965.

9 M. Sakamoto, X. Cai, M. Hara, S. Tojo, M. Fujitsuka and T. Majima, *J. Am. Chem. Soc.*, 2005, **127**, 3702.

10 K. Masuda, M. Nagatomo and M. Inoue, *Nat. Chem.*, 2017, **9**, 207.

11 C. Tang, X. Qiu, Z. Cheng and N. Jiao, *Chem. Soc. Rev.*, 2021, **50**, 8067.

12 (*a*) L. Zheng, W. Zhu, Z. Zhou, K. Liu, M. Gao and B. Z. Tang, *Mater. Horiz.*, 2021, **8**, 3082; (*b*) Z. Zhou, J. Qian, K. Liu, Y. Zhang, M. Gao and B. Z. Tang, *Angew. Chem., Int. Ed.*, 2022, **61**, e202212671.

13 M. Saini, A. Verma, K. Tomar, P. K. Bharadwaj and K. K. Sadhu, *Chem. Commun.*, 2018, **54**, 12836.

14 M. C. Krishna, D. A. Grahame, A. Samuni, J. B. Mitchell and A. Russo, *Proc. Natl. Acad. Sci. U. S. A.*, 1992, **89**, 5537–5541.

15 B. C. Garrett, D. A. Dixon, D. M. Camaioni, D. M. Chipman, M. A. Johnson, C. D. Jonah, G. A. Kimmel, J. H. Miller, T. N. Rescigno, P. J. Rossky, S. S. Xantheas, S. D. Colson, A. H. Laufer, D. Ray, P. F. Barbara, D. M. Bartels, K. H. Becker, K. H. Bowen Jr., S. E. Bradforth, I. Carmichael, J. V. Coe, L. R. Corrales, J. P. Cowin, M. Dupuis, K. B. Eisenthal, J. A. Franz, M. S. Gutowski, K. D. Jordan, B. D. Kay, J. A. LaVerne, S. V. Lymar, T. E. Madey, C. W. McCurdy, D. Meisel, S. Mukamel, A. R. Nilsson, T. M. Orlando, N. G. Petrik, S. M. Pimblott, J. R. Rustad, G. K. Schenter, S. J. Singer, A. Tokmakoff, L. S. Wang and T. S. Zwier, *Chem. Rev.*, 2005, **105**, 355–389.

16 (*a*) J. E. O'Brien, T. B. H. McMurry and C. N. O'Callaghan, *J. Chem. Soc., Perkin Trans. 1*, 1995, 417–420; (*b*) M. N. Elinsona, S. V. Gorbunova, A. N. Vereshchagina, R. F. Nasybullina, A. S. Goloveshkin, I. S. Bushmarinov and M. P. Egorov, *Tetrahedron*, 2014, **70**, 8559–8563; (*c*) S. Yadav, M. Srivastava, P. Rai, J. Singh, K. P. Tiwari and J. Singh, *New J. Chem.*, 2015, **39**, 4556–4561; (*d*) S. Nagaraju, K. Sathish and D. Kashinath, *J. Heterocycl. Chem.*, 2021, **58**, 1252–1258.

17 J. Li, M. J. Lear and Y. Hayashi, *Angew. Chem., Int. Ed.*, 2016, **55**, 9060.

18 J. J. Warren and J. M. Mayer, *J. Am. Chem. Soc.*, 2008, **130**, 7546.

19 E. Buncel, K.-T. Park, J. M. Dust and R. A. Manderville, *J. Am. Chem. Soc.*, 2003, **125**, 5388.

20 M. C. R. Symons, *J. Chem. Soc., Perkin Trans. 2*, 1976, 908.

21 M. Hayyan, M. A. Hashim and I. M. AlNashef, *Chem. Rev.*, 2016, **116**, 3029.

22 X. Ye, L.-H. Chung, K. Li, S. Zheng, Y.-L. Wong, Z. Feng, Y. He, D. Chu, Z. Xu, L. Yu and J. He, *Nat. Commun.*, 2022, **13**, 6116.

23 M. Dharmarwardana, B. M. Otten, M. M. Ghimire, B. S. Arimilli, C. M. Williams, S. Boateng, Z. Lu, G. T. McCandless, J. J. Gassensmith and M. A. Omary, *Proc. Natl. Acad. Sci. U. S. A.*, 2021, **118**, e2106572118.

24 P. Sivaguru, Z. Wang, G. Zanoni and X. Bi, *Chem. Soc. Rev.*, 2019, **48**, 2615.